Near-Infrared Emissive B-N Lewis Pair-Functionalized Anthracenes via Selective LUMO Delocalization in Extended Conjugated Dimer and Polymer

Jingyao Zuo,[a] Kanglei Liu,[a] Jaren Harrell,[a] Lujia Fang,[a] Piotr Piotrowiak,*[a] Daisuke Shimoyama,[a] Roger A. Lalancette,[a] and Frieder Jäkle*[a]

J. Zuo, Dr. K. Liu, Dr. J. Harrell, L. Fang, Prof. Dr. P. Piotrowiak, Dr. D. Shimoyama, Prof. Dr. R. A. Lalancette, Prof. Dr. F. Jäkle

Department of Chemistry, Rutgers The State University – Newark, 73 Warren Street, Newark, NJ 07102, USA

E-mail: piotr@newark.rutgers.edu, fjaekle@newark.rutgers.edu

Abstract

Acenes are attractive as building blocks for low gap organic materials with applications, for example, in organic light emitting diodes, solar cells, bioimaging and diagnostics. Previously, we have shown that modification of dipyridylanthracene via B-N Lewis pair fusion (BDPA) strongly redshifts the emission, while facilitating self-sensitized reactivity toward O_2 to reversibly generate the corresponding endoperoxides. Herein, we report on the further expansion of the π-system of BDPA to a vinyl-substituted monomer, vinylene-bridged dimer, and a polymer with an average of 20 chromophores. The extension of π-conjugation results in largely reduced band gaps of 1.8 eV for the dimer and 1.7 eV for the polymer, the latter giving rise to NIR emission with a maximum at 731 nm and an appreciable quantum yield of 7%. Electrochemical and computational studies reveal efficient delocalization of the lowest unoccupied molecular orbital (LUMO) along the pyridyl-anthracene-pyridyl axis, which results in effective electronic communication between BDPA units, selectively lowers the LUMO, and ultimately narrows the band gap. Time-resolved emission and transient absorption (TA) measurements offer insights into the pertinent photophysical processes. Extension of π-conjugation also slows down the self-sensitized formation of endoperoxides, while significantly accelerating the thermal release of singlet oxygen to regenerate the parent acenes.

Introduction

Low band gap chromophores that exhibit NIR absorption or emission are of high demand in organic electronics, including photovoltaics, photodetectors, and light emitting devices, as well as in the biomedical field, because of the ability of NIR light to readily penetrate tissues.[1] A straightforward strategy for tuning the HOMO-LUMO gap in pursuit of low band gap materials is to extend the π-conjugation length.[2] Extension of organic π-conjugated materials typically leads to simultaneous elevation of the HOMO and lowering of the LUMO levels (Figure 1a, **A**). While this approach results in reduced band gaps, the elevation of the HOMO can be deleterious to the oxidative stability of organic π-conjugated materials. In contrast, tricoordinate boron has been shown to facilitate extension of π-conjugation with ensuing reduced band gaps via overlap of the unoccupied p_z orbital on boron with antibonding p* orbitals of adjacent organic p-systems (Figure 1a, **B**).[3] Largely reduced band gaps have also been achieved by linking together tetracoordinate boron complexes, such as dipyrromethenes (BODIPYs, **C**)[4] or boron formazanates (**D**)[5] to generate conjugated dimers, oligomers, and polymers (Figure 1b).[6] Boron-doped π-conjugated polymers are attractive as pivotal components in electronic and optoelectronic devices,

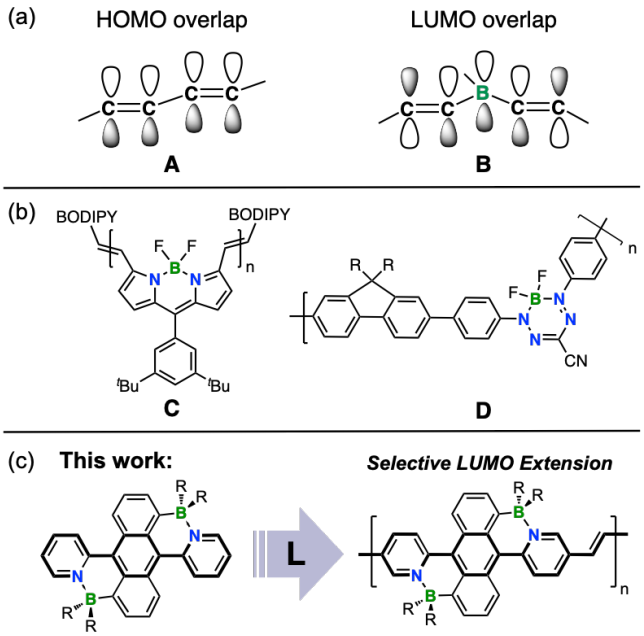

Figure 1. (a) Extension of conjugation in traditional organic π-conjugated polymers and tricoordinate organoboron polymers; (b) tetracoordinate boron polymers; (c) selective "LUMO extension" of B-N Lewis pair-fused anthracenes.

including polymer-based organic light-emitting diodes (OLEDs), field-effect transistors (OFETs), and photovoltaics (OPVs), chemical sensors, and the development of new luminescent materials for imaging applications.[3, 7]

Heteroatom incorporation into polycyclic aromatic hydrocarbons (PAHs) presents a promising approach to modify their electronic structure and to tune the properties for applications in organic electronics, luminescent materials, biomedical applications, and catalysis science.[8] By replacing C-C for isoelectronic and isosteric B-N units desirable

electronic structures and properties can be realized, such as, electron-transporting characteristics, low-lying LUMO orbitals, redshifted absorptions and emissions reaching into the NIR, and thermally activated delayed fluorescence (TADF).[9] In addition, the core of PAHs can be deliberately distorted and helical structures can be generated readily by introducing B-N units, thereby altering the reactivity, photophysical and optoelectronic properties.[10]

In prior work, our group has explored the functionalization of PAHs with B-N Lewis pairs as a mean to tune their optoelectronic properties.[11],[12] Investigations of B-N Lewis pair functionalized anthracenes (BDPAs) showed that the LUMO levels exhibit a pronounced quinoidal character with contributions from the central anthracene ring and the pyridyl moieties.[11a, b] This suggested that extension of conjugation through polymerization at the pyridyl sites may further lower the LUMO levels, while leaving the HOMO levels unaffected,[6f, 13] resulting in a decrease in the HOMO-LUMO gap through "LUMO extension" (Figure 1b). Herein we discuss the effect of extending the conjugated structure of B-N Lewis pair-substituted anthracenes (BDPA) from monomer to dimer and polymer with vinyl bridges on the optoelectronic properties and reactivity toward oxygen. We demonstrate that selective extension of π-conjugation at the LUMO level results in effective electronic communication between BDPA units, narrowed band gaps, and strong luminescence in the NIR region. We also investigate the effect of extension of π-conjugation on the self-sensitized reactivity toward oxygen and the thermal release of singlet oxygen from the corresponding endoperoxides.

Results and Discussion

Synthetic Approach and Structural Features

The synthesis of the vinyl-substituted monomer (**BDPA-Vi2**), the vinylene-bridged dimer (**BDPA2-Vi**), and the vinylene-BDPA alternating copolymer (**PBDPA**) starts from monobrominated (**DPA-Br**) and dibrominated (**DPA-Br2**) 9,10-dipyridylanthracene. As detailed in the Supporting Information (SI), **DPA-Br2** was obtained readily by Suzuki-Miyaura coupling of 9,10-bis(pinacolboryl)anthracene and 2,5-dibromopyridine in 80% yield. A stepwise synthesis with initial introduction of an unsubstituted pyridyl group, followed by coupling of the resultant 9-pyridyl-10-(pinacolboryl)anthracene with 2,5-dibromopyridine, furnished the mono-brominated **DPA-Br** in an overall yield of 41%. Nitrogen-directed electrophilic borylation[14] of **DPA-Br2** and **DPA-Br** was then accomplished according to a previously established protocol[11a, b] by sequential addition of BCl_3 (4 equiv.), 2,6-di-*tert*-butylpyridine (DBP, 2 equiv.), $AlCl_3$ (4 equiv.), followed by quenching of the borenium ion intermediate with Bu_4NCl (Scheme 1). The obtained dichloroborylated Lewis pair complexes were converted *in situ* to the diethylboryl derivatives by treatment with diethyl zinc. Purification by column chromatography (under nitrogen protection and in the dark to avoid photo-induced endoperoxide formation) and recrystallization furnished **BDPA-Br2** and **BDPA-Br** as red-colored crystalline solids in 51% and 58% yield respectively. A dibrominated derivative with octyl groups on boron (**BDPAO-Br2**) was generated in a similar manner from **DPA-Br2**, except for the use of trioctylaluminum instead of diethyl zinc, and isolated as a red oil in 32% yield after column chromatography.

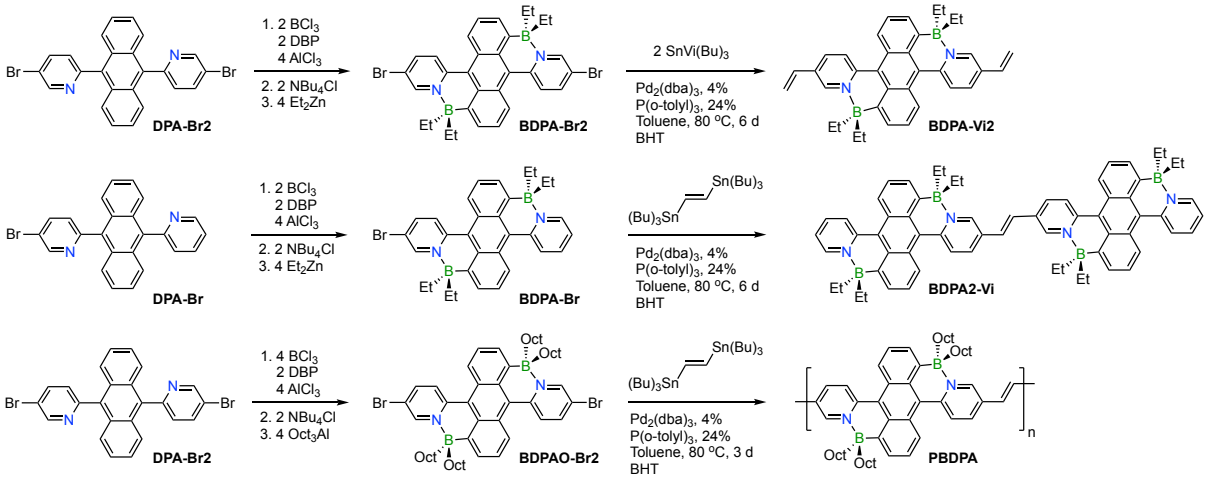

Scheme 1. Synthesis of vinyl-functionalized monomer **BDPA-Vi2**, dimer **BDPA2-Vi**, and polymer **PBDPA**; DBP = 2,6-di-*tert*-butylpyridine, BHT = butylated hydroxytoluene (2,6-dimethyl-4-*tert*-butylphenol)

Having the brominated B-N Lewis pair complexes in hand, we next subjected them to Stille coupling with the respective vinyl tin species as illustrated in Scheme 1. Coupling of **BDPA-Br2** with tri(*n*-butyl)vinyltin furnished **BDPA-Vi2** which was isolated in the form of purple crystals in 75% yield after filtration through a plug of silica gel and recrystallization from a mixture of DCM and hexanes (v/v = 1:1) at -20 ºC. The dimer **BDPA2-Vi** was synthesized in a similar manner from **BDPA-Br** and *trans*-1,2-bis(tributylstannyl)ethene. Silica gel column chromatography and extensive washing, first with hexanes and then with a mixture of hexanes and DCM (v/v = 10/1), gave the pure product as a navy-blue powder in 32% yield. The structures of **BDPA-Vi2** and **BDPA2-Vi** were ascertained by multinuclear and two-dimensional NMR, including 2D H,H-COSY and H,H-NOESY, as well as high-resolution APCI-MS analysis. The boron atoms resonate at 0.0 and 0.1 ppm respectively, which is in the typical range for such tetracoordinate complexes,[11a, b] and the vinylene units give rise to the expected set of 3 multiplets at 6.84, 5.99, 5.59 ppm for **BDPA-Vi2** and a singlet at 7.38 ppm for **BDPA2-Vi**.

When attempting to prepare a polymer by Stille coupling of **BDPA-Br2** and *trans*-1,2-bis(tributylstannyl)ethene, the product showed poor solubility in all common solvents. A more soluble polymer was obtained by Stille coupling of *trans*-1,2-bis(tributylstannyl)ethene and octyl-substituted **BDPAO-Br2** which was prepared in a similar manner as **BDPA-Br2**. The polymer was precipitated in methanol twice and collected by centrifugation. To remove lower molecular weight oligomers that may affect the optoelectronic properties the collected product was washed first with pentane and then with cyclohexane overnight. The pure polymer **PBDPA** was obtained as a dark blue powder in 56% yield. The structure of the polymer was confirmed by multinuclear NMR spectroscopy. The ^{11}B NMR spectrum shows a resonance at -2.3 ppm which is close to that of the respective monomer (0.6 ppm) and confirms the incorporation of intact B-N Lewis pair complexes into the polymer chains. Broad signals in the aromatic region between 7.5 – 9.0 ppm can be assigned to the anthracene and pyridyl units, relying on H,H-COSY correlations and comparisons to data for the monomer, while the signal for the vinylene linker is identified at 7.39 ppm, close to that of the dimer, **BDPA2-Vi**, at 7.38 ppm.

The structural features of the BDPA building block were studied by X-ray diffraction.[15] Single crystals of vinylated **BDPA-Vi2**, the brominated precursor **BDPA-Br2**, and the

methylated reference system **BDPA-Me2**[11b] were grown from DCM/hexanes mixture at -20 ºC. Despite our best efforts, suitable single crystals could not be obtained for dimer **BDPA2-Vi**. The molecular structure of **BDPA-Vi2** is depicted in Figure 2a and those of **BDPA-Br2** and **BDPA-Me2** in Figure S54 (SI). The relevant structural parameters are summarized in Table S1 (SI). The B-N distances for **BDPA-Br2** (1.634(2) Å), **BDPA-Me2** (1.633(2), 1.626(2) Å), and **BDPA-Vi2** (1.631(4) Å) are in the typical range, indicating strong Lewis acid-base interactions. As seen previously for related complexes,[11a, b] the Lewis pair (LP) formation leads to a buckled anthracene backbone with large interplanar angles between the outer benzene rings of 21.8° for **BDPA-Br2**, 22.7° for **BDPA-Me2**, and 20.6° for **BDPA-Vi2**. By comparing the structure of **BDPA-Vi2** with those of **BDPA-Me2** and **BDPA-Br2** (and other reported analogs[11a, b]), it is evident that the Cent1-C1-B angle β = 171.2º is relatively closer to 180º in **BDPA2-Vi** (**BDPA-Me2**, β = 167.9, 168.7º; **BDPA-Br2**, β = 167.7, 168.9º), as is the Cent2-C2-C_{Py} angle of γ = 169.2º (**BDPA-Me2**, γ = 166.2, 166.3º; **BDPA-Br2**, γ = 165.7, 166.1º), see Figure 2. Furthermore, the interplanar angle between the inner anthracene ring and the pendent pyridyl groups of ϕ = 30.1º is significantly smaller for **BDPA-Vi2** (**BDPA-Me2**, ϕ = 39.4, 38.8º; **BDPA-Br2**, ϕ = 38.7º). Thus, the X-ray crystal structure shows that **BDPA-Vi2** adopts a more planar molecular conformation, which should promote electronic delocalization also in the further extended polymeric system.

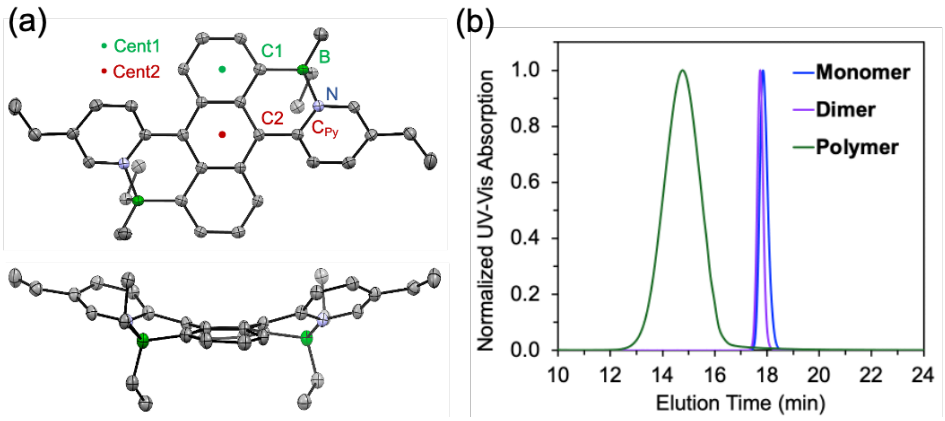

Figure 2. (a) Views of the X-ray crystal structure of **BDPA-Vi2** (thermal ellipsoids at 50% probability); (b) GPC-PDA data for monomer **BDPA2-Vi**, dimer **BDPA2-Vi**, and polymer **PBDPA** in THF (1 mL min^{-1}).

The number-average molecular weight of the purified polymer was estimated by gel permeation chromatography (GPC) in THF relative to narrow polystyrene standards to be M_n = 16,900 ($Đ$ = 1.50), corresponding to an average degree of polymerization of DP_n = 20. GPC with photodiode array (PDA) detection revealed an absorption maximum at λ = 662 nm for low molecular weight polymers (extracted at an elution time of 16.5 min), while that of high molecular weight polymers at the limit of π-extension (extracted at 13.7 min) was determined to be λ = 684 nm (Figure 2b; see also Figure S52, SI). The latter is close to the absorption maximum of the isolated polymer sample at λ = 676 nm.

Effects of π-Extension on Electronic Structure

To examine the effects of extension of π-conjugation at the pyridyl sites on the electronic structure we first conducted DFT calculations on the monomer **BDPA-Vi2** and the dimer **BDPA2-Vi**, and compared the results with those for the methylated derivative **BDPA-Me2**[11b] (Figure 3). As also seen in the X-ray structure, the vinyl groups of **BDPA-Vi2** are positioned at a slight dihedral angle of 14.7º relative to the pyridyl moieties, whereas the Py-Vi-Py linker unit for **BDPA2-Vi** adopts an almost perfectly coplanar arrangement (3.7º; see Figure S55, SI). Hence, we anticipated that orbital delocalization into the vinyl groups for the monomer and the vinylene bridge for the dimer should strongly influence the LUMO energies and the HOMO-LUMO gap. For **BDPA-Vi2**, the HOMO is localized primarily on the anthracene moiety and only very slightly shifts with extension of the conjugated system (Table S3, SI). In contrast, the LUMO is cross-conjugated and extensively delocalized into the pyridyl and vinyl groups. For the dimer **BDPA2-Vi** the HOMO and HOMO-1 represent linear combination of orbitals localized on each of the acene sub-units, whereas the LUMO and LUMO+1 are cross-conjugated and localized predominantly on the vinylene linker and the C-C bonds between anthracene and pyridyl groups respectively (Figure 3b). Owing to the significant lowering of the LUMO levels from -2.51 to -2.78 eV and -3.05 eV, the computed energy gap decreases in the order **BDPA-Me2** (2.30 eV) > **BDPA-Vi2** (2.06 eV) > **BDPA2-Vi'** (1.83 eV). Thus, the reduction in the HOMO-LUMO gap is correlated with and rooted in the orbital delocalization involving the vinylene units. It is reasonable to assume that further extension to the polymer **PBDPA** results in even more extensive delocalization of the LUMO, involving the vinylene bridges and pyridyl groups, and a further reduction in the energy gap.

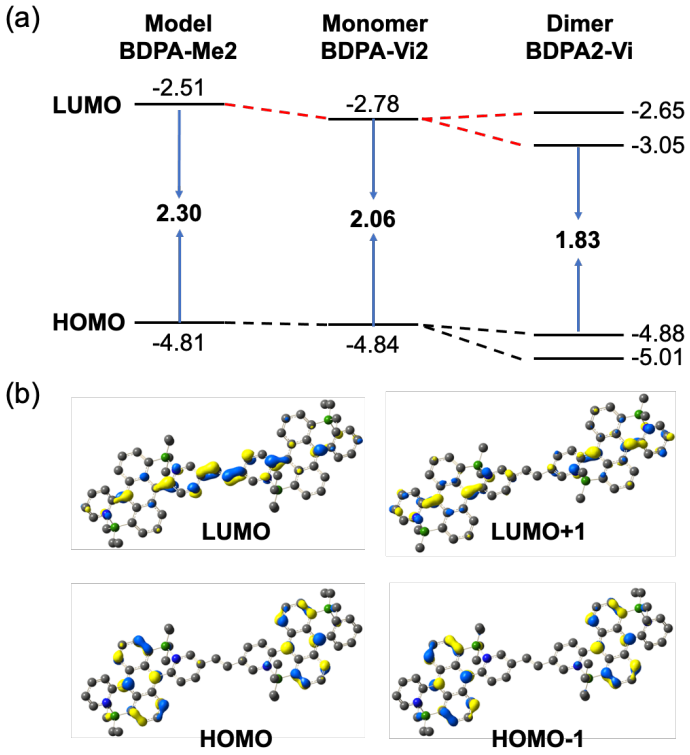

Figure 3. (a) Depiction of the frontier orbital energy levels for monomer **BDPA-Vi2** and dimer **BDPA2-Vi**, in comparison to **BDPA-Me2**; (b) plots of computed Kohn-Sham HOMO/HOMO-1 and LUMO/LUMO+1 orbitals for **BDPA2-Vi**.

To further investigate the electronic structures, cyclic voltammetry (CV) and square wave voltammetry (SWV) measurements were performed in DCM solution containing 0.1 M $Bu_4N[PF_6]$ as the supporting electrolyte (molecular compounds), as well as for a thin film of the polymer in acetonitrile containing 0.1 M $Bu_4N[PF_6]$ (Figure 4). For **BDPA-Vi2** and **BDPA2-Vi** two and four consecutive reversible reduction processes could be resolved respectively. The pronounced redox splitting of 170 mV between the first and second reduction process for **BDPA-Vi2** (-1.61, -1.78 V) indicates that initially one electron is injected and then a second one at a more negative potential. For the dimer **BDPA2-Vi**, two waves occur at -1.52, -1.64 V, followed by two additional waves at more negative potentials of -1.89, -2.04 V. The redox splitting between the first two waves of 120 mV and the third and fourth wave of 150 mV is overall similar though slightly less pronounced than for **BDPA-Vi2**. Relative to the potentials for the first and second reduction, those for the third and fourth reduction are much more negative by 370 and 400 mV respectively. The polymer shows a very broad feature that extends over the entire range from ca. -1.4 to -2.2 V vs $Fc^{+/0}$, indicating the presence of multiple overlapping redox waves. Importantly, the first reduction becomes increasingly less negative when going from the monomer ($E_{1/2}$ = -1.52 V) to the dimer ($E_{1/2}$ = -1.47 V) and the polymer ($E_{red,\ onset}$ = -1.40 V). This further confirms that electronic communication between individual BDPA units across the vinylene linker is strong, which is consistent with the extensive delocalization of the LUMO predicted by the DFT calculations. Oxidative scans acquired in DCM containing 0.1 M $Bu_4N[PF_6]$ showed irreversible redox processes with onset potentials of $E_{ox,\ onset}$ = 0.36 V (monomer), 0.37 V (dimer), and 0.31 V (polymer) (and Figure S56, SI). The electrochemical gaps derived from the cyclic voltammetry data of 1.88, 1.84, and 1.71 eV for the monomer, dimer, and polymer compare well with the optical gaps deduced from UV-Vis absorption spectra of 1.94, 1.84, and 1.70 eV (*vide infra*). These results further indicate that extension of conjugation through the pyridyl side groups and vinylene linkers is very effective and leads to gradually decreasing LUMO levels and HOMO-LUMO gaps.

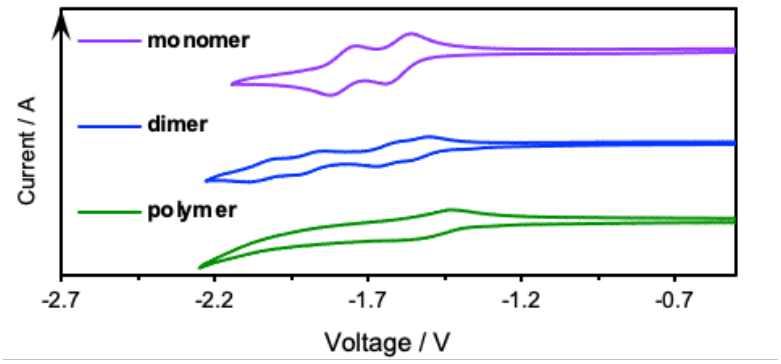

Figure 4. Reductive scans of cyclic voltammograms in DCM solution containing 0.1 M $Bu_4N[PF_6]$ (scan rate 250 mV s^{-1}; reported relative to Fc/Fc^+).

Table 1. Cyclic voltammetry data and comparison of electrochemical HOMO-LUMO gaps with results from DFT calculations and UV-Vis absorption spectroscopy.[a]

Compound	$E_{ox,\ CV}$ [a]	$E_{red,\ CV}$ [a]	HOMO [b]	LUMO [b]	$E_{g,\ CV}$ [b] (eV)	$E_{g,\ DFT}$ [c] (eV)	$E_{g,\ opt}$ [d] (eV)
BDPA-Me2 [11b]	0.32	-1.61	-4.72	-2.79	1.93	2.30	2.05
BDPA-Vi2	0.36	-1.52	-4.76	-2.88	1.88	2.06	1.94
BDPA2-Vi	0.37	-1.47	-4.77	-2.93	1.84	1.83	1.84
PBDPA	0.31	-1.40	-4.71	-3.00	1.71	N/A	1.70

[a] Onset oxidation and reduction potentials, recorded using 0.1 M $Bu_4N[PF_6]$ in DCM. [b] Determined from CV data using the equations E_{LUMO} = -(4.4 + E_{red}) and E_{HOMO} = -(4.4 + E_{ox}). [c] From DFT calculations at the RB3LYP/6-31G(d) level of theory. [d] Estimated from onset of absorption in DCM solution.

Effects of π-Extension on Photophysical Properties

The absorption and emission spectra in DCM solution are displayed in Figure 5, and the photophysical properties are summarized and compared with data for the methylated model system **BDPA-Me2**[11b] in Table 2. Extension of π-conjugation along the dipyridyl axis results in strong bathochromic shifts of the absorption and emission bands. The wavelength of the absorption maximum shifts from 555 nm (**BDPA-Me2**) to 676 nm (**PBDPA**), and the wavelength of the emission maximum shows a similar trend, reaching to 731 nm for the polymer. TD-DFT data for the monomer **BDPA-Vi2** indicate that the lowest energy absorption arises from a HOMO-to-LUMO transition to a cross-conjugated state. For the dimer **BDPA2-Vi**, both HOMO-to-LUMO and HOMO-1-to-LUMO+1 transitions are predicted to contribute to the lowest energy absorption with the LUMO more localized on the vinylene linker and the LUMO+1 on the C-C bonds between anthracene and pyridyl groups (*see* Figure 3b and Table S4, SI).

The emission for **BDPA-Vi2** is relatively long-lived (τ_{Fl} = 8.3 ns) and very intense, giving a quantum yield of ϕ_{Fl} = 74% that is almost twice that of **BDPA-Me2** (43%, 10.2 ns). Upon extension to the dimer (12%, 0.58 ns) and polymer (7%, 0.65 ns), the quantum yield decreases and the lifetime becomes significantly shorter, which is likely due to a combination of the lower band gap, the greater molecular flexibility, and possibly also increasingly favorable intersystem crossing (ISC) to the triplet manifold as the singlet-triplet gap becomes much smaller (Table S5 and Figure S73, SI). This is reflected in a corresponding increase in the nonradiative decay rate constant (k_{nr}) from the monomer (3.1×10^7 s^{-1}) to the dimer (152×10^7 s^{-1}) and polymer (143×10^7 s^{-1}) that largely outweighs slight changes in the radiative decay rate constant (k_r).[16]

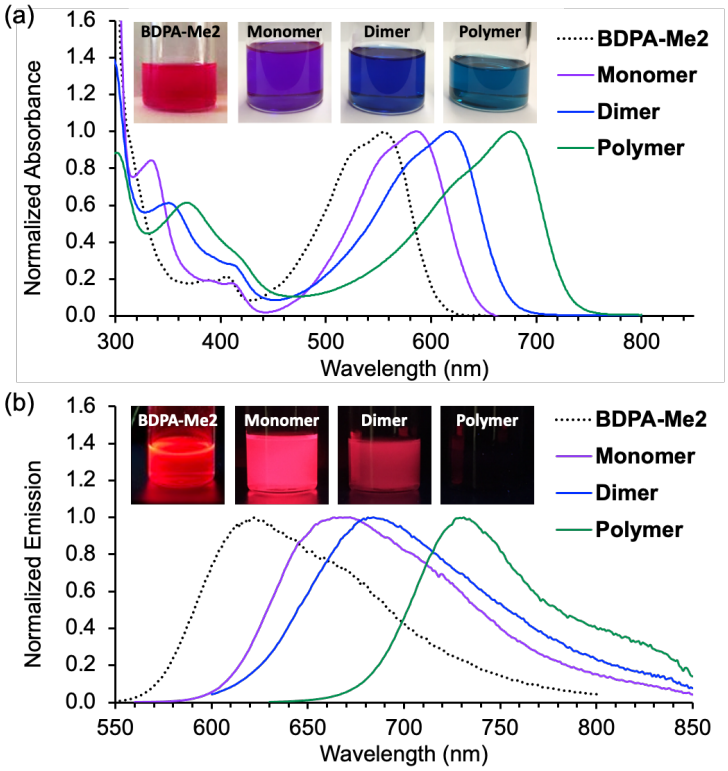

Figure 5. (a) UV-vis absorption and (b) emission spectra of **BDPA-Me2**, monomer **BDPA-Vi2**, dimer **BDPA2-Vi**, and polymer **PBDPA** in DCM solution; insets show photographs under (a) natural light and (b) UV irradiation at 365 nm. **Table 2.** Results from photophysical studies in DCM solution.

Table 2. Results from photophysical studies in DCM solution

Compound	λ_{abs} / nm	$\lambda_{abs,TDDFT}$ / nm	λ_{Fl} [a] / nm	ϕ_{Fl} [b] / %	τ_{Fl} [c] / ns	k_r/k_{nr} [d] / 10^7 s^{-1}
BDPA-Me2 [11b]	555	532	622	43	10.2 [e]	4.2/5.6
BDPA-Vi2	585	560	672	74	8.3 [e]	8.9/3.1
BDPA2-Vi	617	615	684	12	0.58 [f]	20.7/152
PBDPA	676	N/A	731	7	0.65 [g]	10.8/143

[a] Excited at longest wavelength absorption maximum. [b] Absolute quantum yield determined with an integrating sphere. [c] Fluorescence lifetime. [d] Radiative (k_r) and non-radiative (k_{nr}) decay rate constants calculated using the equations $k_r = \Phi / \tau$, $k_{nr} = (1 - \Phi) / \tau$). [e] Excited with a nanoLED at λ_{exc} = 450 nm. [f] λ_{exc} = 670 nm; major component of double-exponential fit with τ_1 = 0.58 ns (96.5 %), τ_2 = 5.6 ns (3.5 %). [g] λ_{exc} = 670 nm; major component of double-exponential fit with τ_1 = 0.65 ns (96.3 %), τ_2 = 3.8 ns (3.7 %); the small longer-lived component is likely due to traces of partially oxidized species (endoperoxide formation on one of the two acenes), see Figure S76.

The dependence of the UV-Vis and fluorescence properties of **BDPA-Vi2** and **BDPA2-Vi** on the solvent polarity was also examined by acquiring data in toluene, dichloromethane, and acetonitrile – the polymer was not studied due to poor solubility in non-polar solvents (Figure S61-S62, SI). The absorption maximum of both compounds experiences a modest hypsochromic shift with increasing solvent polarity that is more pronounced for **BDPA2-Vi** (solvatochromic shift of 993 cm^{-1}) than **BDPA-Vi2** (solvatochromic shift of 760 cm^{-1}). The emission spectra present a similar trait, again the more polar solvent acetonitrile gives rise to a blue-shifted emission relative to that in DCM or toluene.[17] The emission maximum of **BDPA2-Vi** shifts by 374 cm^{-1} while that of **BDPA-Vi2** shifts by 298 cm^{-1} in acetonitrile relative to toluene solution. This may indicate that more polar solvents lead to less effective π-delocalization and symmetry-breaking in the excited state due to a more twisted molecular structure.

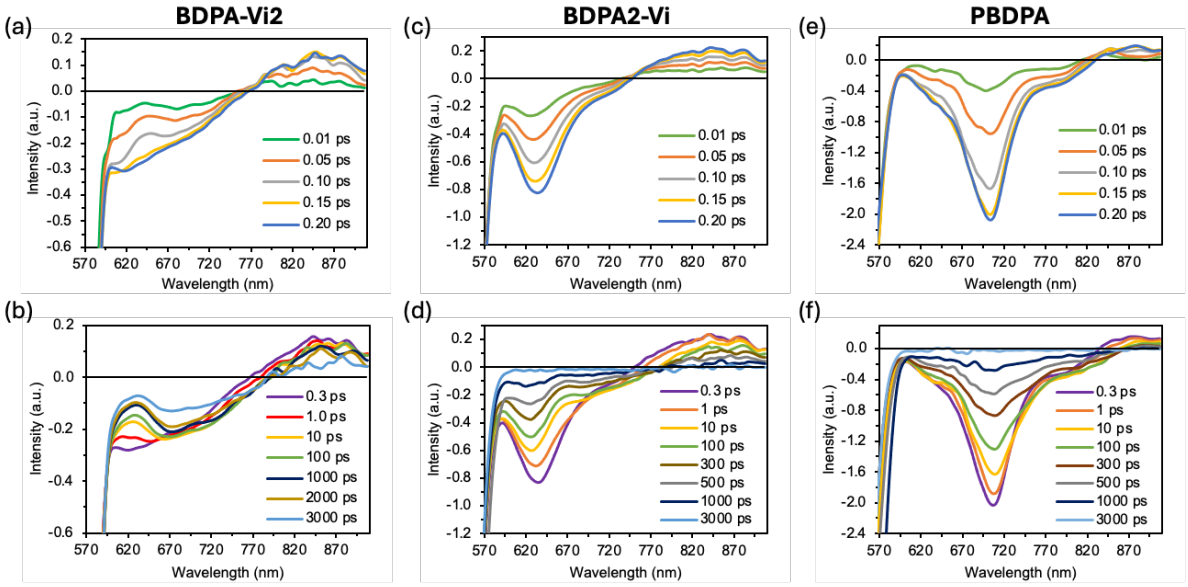

Figure 6. Transient absorption (TA) spectra of (a,b) **BDPA-Vi2**, (c,d) **BDPA2-Vi**, and (e,f) **PBDPA** at different time delays in de-aerated DCM (λ_{exc} = 550 nm).

To gain further insights into the nature of the photo-excited states, femtosecond-transient absorption (fs-TA) spectroscopy was performed on the monomer **BDPA-Vi**, dimer **BDPA2-Vi**, and polymer **PBDPA**. Figure 6 shows plots of the TA spectra for **BDPA2-Vi** and **PBDPA** in de-aerated DCM, following excitation at 550 nm (Figures S68-S70, SI). At short time delays, a strong negative signal arises at 600 nm for the monomer, 630 nm for the dimer, and 700 nm for the polymer, which is attributed to their ground state bleaching (GSB) and signifies formation of excited molecules. An additional negative shoulder at ~660 nm for the monomer, ~690 nm for the dimer, and ~780 nm for the polymer denotes stimulated emission (SE). The SE of **BDPA-Vi2** becomes more prominent at 1000 ps as ground state repopulation occurs and lasts longer than for **BDPA2-Vi** and **PBDPA**, which barely show any remaining SE beyond 1000 ps. The longer lasting SE for **BDPA-Vi2** is consistent with its relatively longer florescence lifetime and higher photoluminescence quantum yield. The positive bands at short wavelength of 540 to 560 nm and longer wavelengths of 770 to 900 nm for **BDPA-Vi2**, 780 to 900 nm for

BDPA2-Vi, and 860 to 900 nm for **PBDPA** are attributed to $S_1 \rightarrow S_n$ excited state absorptions (ESA). Absorptions from triplet excited states could not be detected as they likely occur at longer wavelengths beyond the detection limit of our set up. Some band shifting of the GSB to lower energy with increasing delay time as the signal is rising was apparent in the TA spectra of **BDPA2-Vi** and **PBDPA** but mostly absent for **BDPA-Vi2**. This feature may originate from the solvent polarity dependence of the absorption of these molecules. As discussed earlier, the ground state UV-Vis spectra in toluene, DCM and acetonitrile revealed a moderate negative solvatochromic effect (bathochromic shift in less polar solvent).

It is also possible that for the dimeric (and polymeric species) a more delocalized excited state is initially accessed which then decays via a more localized excited state.[18] To further assess this possibility, calculations were performed that revealed the existence of three distinct rotamers of the **BDPA2-Vi** dimer which correspond to different orientation of the B-N bonds with respect to the central >C=C< bridge (Figure S71). In the ground state the energy differences between the ∥∥ (parallel-parallel), ∥⊥ (parallel-perpendicular) and ⊥⊥ (perpendicular-perpendicular) rotamers are small. Not accounting for solvation, the relative populations are predicted as 58% ∥∥, 35% ∥⊥ and 7% ⊥⊥. The calculated ground state absorption spectra indicate distinct peak positions and features for the three rotamers. As seen in Figure S72, the well-defined ⊥⊥, ∥⊥ and ∥∥ rotamer minima persist in the optimized structures of the S_1 and T_1 states. As a result, upon reaching the S_1 state, the initially excited distribution of rotamers determined by the overlap between the pump pulse and the ground state absorption spectra, must undergo equilibration reflecting both the gas phase energies as well as solvation (the latter favors the ∥⊥ rotamer because of its residual dipole moment). The equilibration of rotamers in the S_1 state is a likely contributor to the spectral evolution of the transient absorption spectra observed for the **BDPA2-Vi** dimer at longer time scales. Similar long-time scale spectral evolution is not observed in the transient absorption spectra of the **PBDPA** polymer because the rotation of the monomeric is hindered, except for the termini of the strand.

Effects of π-Extension on Singlet Oxygen Sensitization

We previously disclosed that an unusual feature of B-N fused anthracenes, such as **BDPA-Me2,** is their efficient self-sensitized reactivity with oxygen to generate the corresponding endoperoxides from which singlet oxygen can then be thermally released.[11b] Singlet oxygen plays an important role in numerous fields, including organic synthesis, photodynamic therapeutic (PDT) treatment of cancer,[19] and material science[20]. This prompted us to further investigate the effect of extending the π-conjugation on the reactivity toward and release of oxygen. Solutions in oxygen-saturated DCM (2×10^{-5} M) were irradiated with a Xe lamp at room temperature (Figure 7a and Figures S74-S75, SI) as detailed in the SI. The kinetic study revealed a strong influence of extension of conjugation through the pyridyl side groups: **BDPA-Vi2** reacted over two orders of magnitude more slowly than **BDPA-Me2**. Upon extension of conjugation from **BDPA-Vi2** to the dimer **BDPA2-Vi** the reaction rate diminished further, and the polymer **PBDPA** proved to be most resistant to autooxidation under irradiation with white light of >455 nm (Figure 7a). In previous works, differences in HOMO energy had been linked to differences in the reactivity of acenes toward oxygen,[11a, b] and for B-N Lewis pair functionalized anthracenes electron-withdrawing substituents on boron were shown to significantly reduce the rate of autooxidation.[11d] However, as discussed above, the HOMO levels are fairly similar in energy for all these compounds, and so is the absorptivity per B-N

Lewis pair-fused anthracene moiety (Table S2, SI). Furthermore, the energy gap between singlet ground state and triplet excited state decreases in the order **BDPA2-Vi** >> **BDPA-Me2** > **BDPA-Vi2** and the triplet levels are close to or above the energy gap between singlet and triplet oxygen of 94.3 kJ mol^{-1} in all cases (Table S5, SI).[11b] A possible alternative explanation is that this effect is related to the more delocalized spin density as illustrated for the monomer and dimer in Figure S73, SI. However, the origin of the enhanced stability of the vinyl monomer, dimer, and polymer toward autooxidation in comparison to the methyl derivative remains not fully understood.

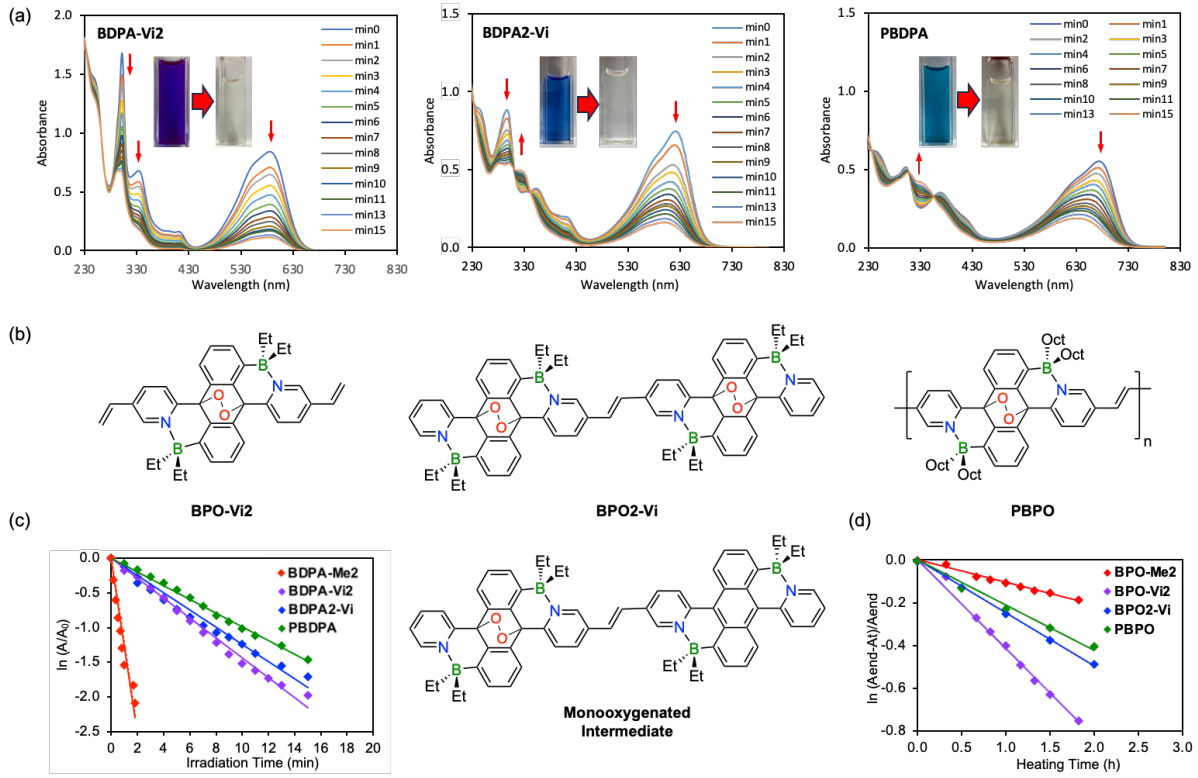

Figure 7. (a, b) UV-vis spectra at different times for the reaction of BN-functionalized anthracenes (0.02 mM "anthracene units" in oxygen-saturated DCM) with oxygen upon photoirradiation by a Xe lamp (34 Watt, a cutoff filter of 455 nm was used) at room temperature to give the respective endoperoxides. (c) Pseudo first-order kinetics for the reaction of **BDPA-Me2**, **BDPA-Vi2**, **BDPA2-Vi** and **PBDPA** with oxygen upon photoirradiation to give the respective endoperoxides in DCM (455 nm cut-off filter was applied; **BDPA-Me2**: k_{app} = 1200 × 10^{-3} s^{-1}; **BDPA-Vi2**: k_{app} = 2.4 × 10^{-3} s^{-1}; **BDPA2-Vi**: k_{app} = 2.1 × 10^{-3} s^{-1}; **PBDPA**: k_{app} = 1.6 × 10^{-3} s^{-1}). (d) Kinetics for the thermolysis of the endoperoxides at 100 °C in toluene (0.1 mM "anthracene units"). A_{end}: final absorption intensity of regenerated acene; A_t: absorption intensity of regenerated acene at a given time (**BPO-Me2**: k_{app} = 2.9 × 10^{-5} s^{-1}; **BPO-Vi2**: k_{app} = 11.2 × 10^{-5} s^{-1}; **BPO2-Vi**: k_{app} = 6.9 × 10^{-5} s^{-1}; **PBPO**: k_{app} = 5.8 × 10^{-5} s^{-1}.

We also studied the ability of the corresponding endoperoxides to thermally revert to the parent acenes with release of singlet oxygen (Figure 7d). Interestingly, the rate of cyclo-reversion for monomer **BPO-Vi2** is almost one order of magnitude higher than that of **BPO-Me2**[11b]. After heating **BPO-Vi2** in toluene at 100 ºC overnight, >90% **BDPA-Vi2** were regenerated according to UV-Vis absorption data, while for **BPO-Me2** only 59% of the parent

acene could be recovered (Figure S78, SI). **BPO2-Vi** also exhibited excellent reversibility, but for the polymer **PBPO** only partial recovery was achieve, possibly due to the occurrence of side reactions. Interestingly, during oxygen release from the endoperoxides, the absorption bands for the dimer and polymer, but not the monomeric species, displayed a gradual redshift with increased heating time (Figure S79, SI). This suggests that the release of singlet oxygen occurs stepwise for the compounds containing multiple endoperoxide units, and that the electronic effect of oxygenated BDPA moieties is distinct from that of the non-oxygenated acenes. Overall, we conclude that replacement of methyl with vinyl groups and the corresponding extension of π-conjugation reduces the tendency for autooxidation but facilitates the reversion of the resulting endoperoxides to the parent acenes through release of singlet oxygen, presumably due to their more favorable planarized geometry and enhanced electronic delocalization.

Conclusion

We have synthesized a series of B-N Lewis pair-functionalized anthracene monomer, model dimer and high molecular weight polymer with vinyl linkers to investigate in detail the electronic structure, the optical properties, and the reactivity toward oxygen upon selective extension of the LUMO conjugation. Single crystal X-ray structures and DFT calculations reveal a more planar geometry for **BDPA-Vi2** in comparison to **BDPA-Me2**, and an almost perfectly coplanar Py-Vi-Py linker for the dimer **BDPA2-Vi**. The extension of conjugation narrows the HOMO and LUMO energy levels and reduces the excited state lifetime because of more rapid non-radiative decay, as evidenced by electrochemical, UV-vis, and time-resolved fluorescence spectroscopy measurements. Nevertheless, an appreciable quantum yield of 7% is measured for the fluorescence of the polymer with a maximum of 731 nm in DCM. The rate of photo-induced reaction with oxygen to give the respective endoperoxides is more than 2 orders of magnitude lower than for **BDPA-Me2** and decreases in the order of **BDPA-Me2** >> **BDPA-Vi2** > **BDPA2-Vi** > **PBDPA**. Conversely, the rate of thermally promoted release of singlet oxygen from the endoperoxides is more favorable, about 4 times faster for **BDPA-Vi2** than **BDPA-Me2**, illustrating its propensity to store and generate singlet oxygen to be potentially useful in photodynamic therapy and other fields where delivery of singlet oxygen on-demand is desirable.

Acknowledgements

F.J. thanks the National Science Foundation (Grants CHE-1954122 and CHE-2247211) and Rutgers University for support. A 500 MHz NMR spectrometer was purchased with support from the State of New Jersey (ELF III 047-04), another 500 MHz NMR spectrometer (MRI-1229030), an X-ray diffractometer (MRI-2018753), and an Orbitrap mass spectrometer (MRI-2215975) with support from the NSF. Supplement funding for this project was provided by the Rutgers University – Newark Chancellor's Research Office. We thank Dr. Pavel Kucheryavy at Rutgers University-Newark for assistance with acquisition of 2D NMR data, Dr. Roman Brukh for assistance with acquisition of mass spectral data, and Dr. Monika Baraniak for assistance with GPC measurements.

References

[1] a) G. Qian, Z. Y. Wang, *Chem. Asian J.* **2010**, *5*, 1006-1029; b) J. Qi, W. Qiao, Z. Y. Wang, *Chem. Rec.* **2016**, *16*, 1531-1548; c) A. Zampetti, A. Minotto, F. Cacialli, *Adv. Funct. Mater.* **2019**, *29*, 1807623; d) J.-B. Li, H.-W. Liu, T. Fu, R. Wang, X.-B. Zhang, W. Tan, *Trends Chem.* **2019**, *1*, 224-234; e) Q. Li, Y. Guo, Y. Liu, *Chem. Mater.* **2019**, *31*, 6359-6379; f) J. Lee, H. Cha, H. Yao, J. Hou, Y.-H. Suh, S. Jeong, K. Lee, J. R. Durrant, *ACS Appl. Mater. Interfaces* **2020**, *12*, 32764-32770; g) B. Li, M. Zhao, J. Lin, P. Huang, X. Chen, *Chem. Soc. Rev.* **2022**, *51*, 7692-7714; h) D. Meng, R. Zheng, Y. Zhao, E. Zhang, L. Dou, Y. Yang, *Adv. Mater.* **2022**, *34*, e2107330; i) X.-Q. Xu, Y. He, Y. Wang, *Cell Rep. Phys. Sci.* **2021**, *2*, 100433; j) H. Li, D. Kim, Q. Yao, H. Ge, J. Chung, J. Fan, J. Wang, X. Peng, J. Yoon, *Angew. Chem. Int. Ed.* **2021**, *60*, 17268-17289; k) C. Yan, Z. Zhu, Y. Yao, Q. Wang, Z. Guo, W.-H. Zhu, *Acc. Mater. Res.* **2024**, *5*, 64-75.

[2] a) G. Wegner, K. Müllen, Eds, VCH, Weinheim, Germany, **1996**; b) A. Tsuda, A. Osuka, *Science* **2001**, *293*, 79-82; c) S. Günes, H. Neugebauer, N. S. Sariciftci, *Chem. Rev.* **2007**, *107*, 1324-1338; d) R. D. McCullough, in *Handbook of Oligo- and Polythiophenes*, Wiley-VCH Verlag GmbH, **2007**, pp. 1-44; e) T. M. Swager, *Macromolecules* **2017**, *50*, 4867-4886.

[3] a) N. Matsumi, K. Naka, Y. Chujo, *J. Am. Chem. Soc.* **1998**, *120*, 5112-5113; b) C. D. Entwistle, T. B. Marder, *Angew. Chem. Int. Ed.* **2002**, *41*, 2927-2931; c) F. Jäkle, *Chem. Rev.* **2010**, *110*, 3985-4022; d) P. K. Chen, R. A. Lalancette, F. Jäkle, *J. Am. Chem. Soc.* **2011**, *133*, 8802-8805; e) K. Tanaka, Y. Chujo, *Macromol. Rapid Comm.* **2012**, *33*, 1235-1255; f) H. Helten, *Chem. Asian J.* **2019**, *14*, 919-935; g) X. Yin, J. Liu, F. Jäkle, *Chem. Eur. J.* **2021**, *27*, 2973-2986.

[4] a) Q. Wu, Z. Kang, Q. Gong, X. Guo, H. Wang, D. Wang, L. Jiao, E. Hao, *Org. Lett.* **2020**, *22*, 7513-7517; b) Q. Wu, Y. Zhu, X. Fang, X. Hao, L. Jiao, E. Hao, W. Zhang, *ACS Appl. Mater. Interfaces* **2020**, *12*, 47208-47219.

[5] Y. Kawano, Y. Ito, S. Ito, K. Tanaka, Y. Chujo, *Macromolecules* **2021**, *54*, 1934-1942.

[6] a) M. Bröring, R. Krüger, S. Link, C. Kleeberg, S. Köhler, X. Xie, B. Ventura, L. Flamigni, *Chem. Eur. J.* **2008**, *14*, 2976-2983; b) A. Wakamiya, T. Murakami, S. Yamaguchi, *Chem. Sci.* **2013**, *4*, 1002-1007; c) J. Ahrens, B. Haberlag, A. Scheja, M. Tamm, M. Bröring, *Chem. Eur. J.* **2014**, *20*, 2901-2912; d) H. Yokoi, S. Hiroto, H. Shinokubo, *Org. Lett.* **2014**, *16*, 3004-3007; e) J. Wang, Q. H. Wu, S. W. Wang, C. J. Yu, J. Li, E. H. Hao, Y. Wei, X. L. Mu, L. J. Jiao, *Org. Lett.* **2015**, *17*, 5360-5363; f) K. Tanaka, *Polym. J.* **2024**, *56*, 61-70; g) L. J. Patalag, L. P. Ho, P. G. Jones, D. B. Werz, *J. Am. Chem. Soc.* **2017**, *139*, 15104-15113; h) D. L. Crossley, L. Urbano, R. Neumann, S. Bourke, J. Jones, L. A. Dailey, M. Green, M. J. Humphries, S. M. King, M. L. Turner, M. J. Ingleson, *ACS Appl. Mater. Interfaces* **2017**, *9*, 28243-28249; i) R. R. Maar, R. Zhang, D. G. Stephens, Z. Ding, J. B. Gilroy, *Angew. Chem. Int. Ed.* **2019**, *58*, 1052-1056; j) J. Wakabayashi, M. Gon, K. Tanaka, Y. Chujo, *Macromolecules* **2020**, *53*, 4524-4532; k) T. Kim, Z. M. Duan, S. Talukdar, C. H. Lei, D. Kim, J. L. Sessler, T. Sarma, *Angew. Chem. Int. Ed.* **2020**, *59*, 13063-13070; l) M. Nakamura, M. Kitatsuka, K. Takahashi, T. Nagata, S. Mori, D. Kuzuhara, T. Okujima, H. Yamada, T. Nakae, H. Uno, *Org. Biomol. Chem.* **2014**, *12*, 1309-1317; m) F. L. Buguis, N. S. Y. Hsu, S. A. Sirohey, M. C. Adam, L. V. Goncharova, J. B. Gilroy, *Chem. Eur. J.* **2023**, *29*, e202302548.

[7] Y. Fan, J. Zhang, Z. Hong, H. Qiu, Y. Li, S. Yin, *Polymers* **2020**, *13*, 75.

[8] a) S. Yamaguchi, K. Tamao, *Chem. Lett.* **2005**, *34*, 2-7; b) X.-M. He, T. Baumgartner, *RSC Adv.* **2013**, *3*, 11334-11350; c) A. Escande, M. J. Ingleson, *Chem. Commun.* **2015**,

51, 6257-6274; d) X. Y. Wang, F. Zhang, K. S. Schellharnmer, P. Machata, F. Ortmann, G. Cuniberti, Y. B. Fu, J. Hunger, R. Z. Tang, A. A. Popov, R. Berger, K. Müllen, X. L. Feng, *J. Am. Chem. Soc.* **2016**, *138*, 11606-11615; e) M. Stępień, E. Gońka, M. Żyła, N. Sprutta, *Chem. Rev.* **2017**, *117*, 3479–3716; f) X. Y. Wang, J. I. Urgel, G. B. Barin, K. Eimre, M. Di Giovannantonio, A. Milani, M. Tommasini, C. A. Pignedoli, P. Ruffieux, X. L. Feng, R. Fasel, K. Müllen, A. Narite, *J. Am. Chem. Soc.* **2018**, *140*, 9104-9107; g) E. von Grotthuss, A. John, T. Kaese, M. Wagner, *Asian J. Org. Chem.* **2018**, *7*, 37-53; h) A. Borissov, Y. K. Maurya, L. Moshniaha, W.-S. Wong, M. Żyła-Karwowska, M. Stępień, *Chem. Rev.* **2022**, *122*, 565-788.

[9] a) A. Wakamiya, T. Taniguchi, S. Yamaguchi, *Angew. Chem. Int. Ed.* **2006**, *45*, 3170-3173; b) D. Li, H. Y. Zhang, Y. Wang, *Chem. Soc. Rev.* **2013**, *42*, 8416-8433; c) A. John, M. Bolte, H. W. Lerner, M. Wagner, *Angew. Chem., Int. Ed.* **2017**, *56*, 5588-5592; d) K. Matsui, S. Oda, K. Yoshiura, K. Nakajima, N. Yasuda, T. Hatakeyama, *J. Am. Chem. Soc.* **2018**, *140*, 1195-1198; e) Y. Min, C. Dou, H. Tian, J. Liu, L. Wang, *Chem. Commun.* **2019**, *55*, 3638-3641; f) S. K. Mellerup, S. Wang, *Trends Chem.* **2019**, *1*, 77-89; g) S. K. Mellerup, S. N. Wang, *Chem. Soc. Rev.* **2019**, *48*, 3537-3549; h) K. Zhao, Z. F. Yao, Z. Y. Wang, J. C. Zeng, L. Ding, M. Xiong, J. Y. Wang, J. Pei, *J. Am. Chem. Soc.* **2022**, *144*, 3091-3098; i) G. Y. Meng, L. J. Liu, Z. C. He, D. Hall, X. Wang, T. Peng, X. D. Yin, P. K. Chen, D. Beljonne, Y. Olivier, E. Zysman-Colman, N. Wang, S. N. Wang, *Chem. Sci.* **2022**, *13*, 1665-1674; j) C. Chen, Y. Zhang, X.-Y. Wang, J.-Y. Wang, J. Pei, *Chem. Mater.* **2023**, *35*, 10277-10294; k) J.-K. Li, M.-Y. Zhang, L. Zeng, L. Huang, X.-Y. Wang, *Angew. Chem. Int. Ed.* **2023**, *62*, e202303093; l) J. Guo, Z. Li, X. Tian, T. Zhang, Y. Wang, C. Dou, *Angew. Chem. Int. Ed.* **2023**, *62*, e202217470; *Angew. Chem.* **2023**, *135*, e202217470; m) C.-L. Deng, A. D. Obi, S. K. Sarkar, B. Y. E. Tra, D. A. Dickie, R. J. Gilliard, *Nat. Chem.* **2024**, *16*, 437.

[10] a) M. Ball, Y. Zhong, Y. Wu, C. Schenck, F. Ng, M. Steigerwald, S. X. Xiao, C. Nuckolls, *Acc. Chem. Res.* **2015**, *48*, 267-276; b) Z. Dominguez, R. Lopez-Rodriguez, E. Alvarez, S. Abbate, G. Longhi, U. Pischel, A. Ros, *Chem.-Eur. J.* **2018**, *24*, 12660-12668; c) J. Full, S. P. Panchal, J. Götz, A.-M. Krause, A. Nowak-Król, *Angew. Chem. Int. Ed.* **2021**, *60*, 4350-4357; d) X. Zhang, F. Rauch, J. Niedens, R. B. da Silva, A. Friedrich, A. Nowak-Król, S. J. Garden, T. B. Marder, *J. Am. Chem. Soc.* **2022**, *144*, 22316-22324; e) C. S. Shen, M. Srebro-Hooper, M. Jean, N. Vanthuyne, L. Toupet, J. A. G. Williams, A. R. Torres, A. J. Riives, G. Muller, J. Autschbach, J. Crassous, *Chem. Eur. J.* **2017**, *23*, 407-418; f) A. Nowak-Król, P. T. Geppert, K. R. Naveen, *Chem. Sci.* **2024**, *15*, 7408-7440.

[11] a) K. L. Liu, R. A. Lalancette, F. Jäkle, *J. Am. Chem. Soc.* **2017**, *139*, 18170-18173; b) K. L. Liu, R. A. Lalancette, F. Jäkle, *J. Am. Chem. Soc.* **2019**, *141*, 7453-7462; c) M. Vanga, R. A. Lalancette, F. Jäkle, *Chem. Eur. J.* **2019**, *25*, 10133-10140; d) M. Vanga, A. Sahoo, R. A. Lalancette, F. Jäkle, *Angew. Chem. Int. Ed.* **2022**, *61*, e202113075; e) K. L. Liu, Z. Q. Jiang, R. A. Lalancette, X. Y. Tang, F. Jäkle, *J. Am. Chem. Soc.* **2022**, *144*, 18908-18917.

[12] a) V. F. Pais, J. M. Lassaletta, R. Fernandez, H. S. El-Sheshtawy, A. Ros, U. Pischel, *Chem.-Eur. J.* **2014**, *20*, 7638-7645; b) V. F. Pais, M. M. Alcaide, R. Lopez-Rodriguez, D. Collado, F. Najera, E. Perez-Inestrosa, E. Alvarez, J. M. Lassaletta, R. Fernandez, A. Ros, U. Pischel, *Chem. Eur. J.* **2015**, *21*, 15369-15376; c) A. C. Shaikh, D. S. Ranade, S. Thorat, A. Maity, P. P. Kulkarni, R. G. Gonnade, P. Munshi, N. T. Patil, *Chem. Commun.* **2015**, *51*, 16115-16118; d) S. P. J. T. Bachollet, D. Volz, B. Fiser, S. Munch, F. Ronicke, J. Carrillo, H. Adams, U. Schepers, E. Gomez-Bengoa, S. Brase, J. P. A. Harrity, *Chem. Eur. J.* **2016**, *22*, 12430-12438; e) J. Huang, Y. Li, *Front. Chem.* **2018**, *6*; f) A. Haque, R.

A. Al-Balushi, P. R. Raithby, M. S. Khan, in *Molecules, Vol. 25*, **2020**; g) J. Huang, X. Wang, Y. Xiang, L. Guo, G. Chen, *Adv. Energy Sustainability Res.* **2021**, *2*, 2100016; h) R. Campos-González, P. Vázquez-Domínguez, P. Remón, F. Nájera, D. Collado, E. Pérez-Inestrosa, F. Boscá, A. Ros, U. Pischel, *Org. Chem. Front.* **2022**, *9*, 4250-4259; i) M. Tasior, P. Kowalczyk, M. Przybył, M. Czichy, P. Janasik, M. H. E. Bousquet, M. Łapkowski, M. Rammo, A. Rebane, D. Jacquemin, D. T. Gryko, *Chem. Sci.* **2021**, *12*, 15935-15946.

[13] K. Tanaka, Y. Chujo, *Chem. Lett.* **2021**, *50*, 269-279.

[14] a) S. A. Iqbal, J. Pahl, K. Yuan, M. J. Ingleson, *Chem. Soc. Rev.* **2020**, *49*, 4564-4591; b) S. Rej, N. Chatani, *Angew. Chem. Int. Ed.* **2022**, *61*, e202209539.

[15] Deposition numbers 2332728 (for **BDPA-Br2**), 2332729 (for **BDPA-Me2**), and 2332730 (for **BDPA-Vi2**) contain the supplementary crystallographic data for this paper. These data are provided free of charge by the joint Cambridge Crystallographic Data Centre and Fachinformationszentrum Karlsruhe Access Structures service.

[16] To rule out any effect of of traces of monomer or other impurities, lifetime measurements of the dimer and polymer were performed at an excitation wavelength of 670 nm, where the monomer does not show any absorbance.

[17] A bathochromic shift of the emission in the solid state for the monomer to 716 nm, dimer to 746 nm, and polymer to 760 nm was also evident (see Figure S60, SI). In the solid state, the quantum yield diminished to 2% for the monomer and 3% for the dimer, and that of the polymer was too low to accurately determine. The weaker emission in the solid state is attributed to aggregation-caused quenching due to the extended π-system and lack of very bulky substituents.

[18] a) M. T. Whited, N. M. Patel, S. T. Roberts, K. Allen, P. I. Djurovich, S. E. Bradforth, M. E. Thompson, *Chem. Commun.* **2012**, *48*, 284-286; b) L. Ma, Z. Kuang, Z. Wang, H. Zhao, Y. Wan, X.-F. Zhang, Y. Li, A. Xia, *J. Phys. Chem. Lett.* **2023**, *14*, 702-708.

[19] a) J. M. Aubry, C. Pierlot, J. Rigaudy, R. Schmidt, *Acc. Chem. Res.* **2003**, *36*, 668-675; b) D. E. J. G. J. Dolmans, D. Fukumura, R. K. Jain, *Nat. Rev. Cancer* **2003**, *3*, 380-387; c) J. F. Lovell, T. W. Liu, J. Chen, G. Zheng, *Chem. Rev.* **2010**, *110*, 2839-2857; d) P. R. Ogilby, *Chem. Soc. Rev.* **2010**, *39*, 3181-3209; e) J. Park, D. W. Feng, S. Yuan, H. C. Zhou, *Angew. Chem. Int. Ed.* **2015**, *54*, 430-435; f) M. A. Filatov, M. O. Senge, *Mol Syst Des Eng* **2016**, *1*, 258-272; g) Y. Qin, L.-J. Chen, F. Dong, S.-T. Jiang, G.-Q. Yin, X. Li, Y. Tian, H.-B. Yang, *J. Am. Chem. Soc.* **2019**, *141*, 8943-8950; h) W. Fudickar, M. Bauch, H. Ihmels, T. Linker, *Chem. Eur. J.* **2021**, *27*, 13591-13604.

[20] a) W. Fudickar, A. Fery, T. Linker, *J. Am. Chem. Soc.* **2005**, *127*, 9386-9387; b) D. Zehm, W. Fudickar, T. Linker, *Angew. Chem. Int. Ed.* **2007**, *46*, 7689-7692; c) S. Martins, J. P. S. Farinha, C. Baleizao, M. N. Berberan-Santos, *Chem. Commun.* **2014**, *50*, 3317-3320; d) M. A. Filatov, S. Karuthedath, P. M. Polestshuk, H. Savoie, K. J. Flanagan, C. Sy, E. Sitte, M. Telitchko, F. Laquai, R. W. Boyle, M. O. Senge, *J. Am. Chem. Soc.* **2017**, *139*, 6282-6285; e) N. Mahne, B. Schafzahl, C. Leypold, M. Leypold, S. Grumm, A. Leitgeb, G. A. Strohmeier, M. Wilkening, O. Fontaine, D. Kramer, C. Slugovc, S. M. Borisov, S. A. Freunberger, *Nat. Energy* **2017**, *2*; f) I. Pibiri, S. Buscemi, A. P. Piccionello, A. Pace, *ChemPhotoChem* **2018**, *2*, 535-547; g) Z. Gao, Y. F. Han, F. Wang, *Nat. Commun.* **2018**, *9*, 3977; h) Y. Q. He, W. Fudickar, J. H. Tang, H. Wang, X. Li, J. Han, Z. Wang, M. Liu, Y. W. Zhong, T. Linker, P. J. Stang, *J. Am. Chem. Soc.* **2020**, *142*, 2601-2608; i) V. Brega, Y. Yan, S. W. Thomas, *Org. Biomol. Chem.* **2020**, *18*, 9191-9209.

[21] Gaussian 16, Revision A.03, M. J. Frisch, G. W. Trucks, H. B. Schlegel, G. E. Scuseria, M. A. Robb, J. R. Cheeseman, G. Scalmani, V. Barone, G. A. Petersson, H. Nakatsuji, X.

Li, M. Caricato, A. V. Marenich, J. Bloino, B. G. Janesko, R. Gomperts, B. Mennucci, H. P. Hratchian, J. V. Ortiz, A. F. Izmaylov, J. L. Sonnenberg, D. Williams-Young, F. Ding, F. Lipparini, F. Egidi, J. Goings, B. Peng, A. Petrone, T. Henderson, D. Ranasinghe, V. G. Zakrzewski, J. Gao, N. Rega, G. Zheng, W. Liang, M. Hada, M. Ehara, K. Toyota, R. Fukuda, J. Hasegawa, M. Ishida, T. Nakajima, Y. Honda, O. Kitao, H. Nakai, T. Vreven, K. Throssell, J. A. Montgomery, Jr., J. E. Peralta, F. Ogliaro, M. J. Bearpark, J. J. Heyd, E. N. Brothers, K. N. Kudin, V. N. Staroverov, T. A. Keith, R. Kobayashi, J. Normand, K. Raghavachari, A. P. Rendell, J. C. Burant, S. S. Iyengar, J. Tomasi, M. Cossi, J. M. Millam, M. Klene, C. Adamo, R. Cammi, J. W. Ochterski, R. L. Martin, K. Morokuma, O. Farkas, J. B. Foresman, and D. J. Fox, Gaussian, Inc., Wallingford CT, 2016.

[22] Y. Zhu, A. R. Rabindranath, T. Beyerlein, B. Tieke, *Macromolecules* **2007**, *40*, 6981-6989.

[23] X. Li, A. Fast, Z. Y. Huang, D. A. Fishman, M. L. Tang, *Angew. Chem. Int. Ed.* **2017**, *56*, 5598-5602.